

Magneto-Thermoelectric Transport in Graphene Quantum Dot with Strong Correlations

Laurel E. Anderson¹, Antti Laitinen¹, Andrew Zimmerman¹, Thomas Werkmeister², Henry Shackleton¹, Alexander Kruchkov^{1,3,4}, Takashi Taniguchi⁵, Kenji Watanabe⁶, Subir Sachdev¹, and Philip Kim^{1,2}

¹*Department of Physics, Harvard University, Cambridge, Massachusetts 02138, USA*


²*Department of Applied Physics, Harvard University, Cambridge, Massachusetts 02138, USA*

³*Department of Physics, Princeton University, Princeton, New Jersey 08544, USA*

⁴*Institute of Physics, École Polytechnique Fédérale de Lausanne, Lausanne, CH 1015, Switzerland
and Branco Weiss Society in Science, ETH Zurich, Zurich, CH 8092, Switzerland*

⁵*Research Center for Materials Nanoarchitectonics, National Institute for Materials Science,
1-1 Namiki, Tsukuba 305-0044, Japan*

⁶*Research Center for Electronic and Optical Materials, National Institute for Materials Science,
1-1 Namiki, Tsukuba 305-0044, Japan*

 (Received 15 January 2024; revised 1 May 2024; accepted 7 May 2024; published 12 June 2024)

Disorder at etched edges of graphene quantum dots (GQD) enables random all-to-all interactions between localized charges in partially filled Landau levels, providing a potential platform to realize the Sachdev-Ye-Kitaev (SYK) model. We use quantum Hall edge states in the graphene electrodes to measure electrical conductance and thermoelectric power across the GQD. In specific temperature ranges, we observe a suppression of electric conductance fluctuations and slowly decreasing thermoelectric power across the GQD with increasing temperature, consistent with recent theory for the SYK regime.

DOI: [10.1103/PhysRevLett.132.246502](https://doi.org/10.1103/PhysRevLett.132.246502)

Strong electronic correlations can generate an emergent system that hosts collective excitations without quasiparticles, deviating from the conventional Fermi liquid picture. One proposed description is the Sachdev-Ye-Kitaev (SYK) model, characterized by random, all-to-all four-body interactions. Originally a model for strange metals and complex quantum phases [1], this model also has been shown to be holographically dual to theories of quantum gravity [2–4], prompting searches for an experimental, solid-state realization of the SYK model [5].

Generating an SYK state requires many electrons at the same energy with random all-to-all interactions. A theoretical proposal suggests creating these conditions by applying an external magnetic field to a graphene quantum dot (GQD) with an irregular boundary [6,7]. The dispersionless nature of Landau levels (LLs) on the lattice allows the electrons inside the GQD to remain nearly degenerate, despite the presence of edge disorder. The irregular shape of the GQD edge causes the electronic wave functions to acquire a random spatial structure, creating random all-to-all interactions between the degenerate fermions in the dot, precisely as needed for the SYK model.

Experimentally, it has been shown that the charge transport across etch-defined GQDs often exhibits the emergence of chaotic dynamics, as a result of the combination of confinement and disorder [8,9]. Detailed theoretical modeling [7] suggests that an etch-defined, nanoscale GQD subjected to quantizing out-of-plane magnetic fields of 10–20 T may host strongly correlated

dynamics reminiscent of the SYK model. Owing to the non-Fermi liquid (NFL) nature of the SYK system, transport through SYK GQDs can produce distinctive characteristic behavior compared to a Fermi liquid (FL) description. For example, nonvanishing extensive entropy in the low-temperature in a SYK quantum dot produces temperature-independent, nonvanishing thermoelectric power (TEP), strongly deviating from the conventional Mott prediction in the FL regime [10]. Electrical conductance fluctuations, which in the FL regime are large and governed by single-particle random matrix theory, are suppressed in the SYK regime, a result of the absence of quasiparticle excitations [11]. Since FL-to-NFL transition in the GQD can be tuned by magnetic field and temperature [12], temperature- and field-dependent transport through the dot can be utilized to investigate the emergence of SYK physics in this system.

In this Letter, we study the interplay of disorder, spatial confinement, and strong electronic interactions in disordered GQD subjected to quantizing magnetic fields of up to 10 T. We measure electrical conductance and TEP across the GQD as a function of temperature, identifying a low-temperature FL phase and high-temperature NFL phase separated by a transition regime. We observe strong suppression of electrical conductance fluctuations and nearly temperature-independent TEP in the NFL regime, consistent with theoretical expectations for the SYK model.

The inset of Fig. 1(a) shows a schematic diagram and electron microscope picture of a GQD used in this Letter. The device consists of *h*-BN-encapsulated monolayer

graphene with top and bottom graphite gates, fabricated using standard polymer stacking techniques [13,14]. We shape the heterostructure into a Hall bar geometry using reactive ion etching, then etch a constriction with a ~ 100 nm diameter island in the center, dividing the active region of the device into two large reservoirs that act as external contacts coupled to the central graphene dot. The top graphite gate above the constriction has been removed to enable independent tuning of the charge carrier densities in the GQD and graphene reservoirs. We note that the bottom graphite is separated from GQD with a thin (5.1 nm) *h*-BN layer in order to reduce the Coulomb charging energy. More details about the device fabrication are provided in the Supplemental Material, Sec. I [15].

The resistance measured across the dot (R_{dot}) is measured by biasing the GQD using the graphene reservoir electrodes. Figure 1(a) shows R_{dot} as a function of the bottom and top graphite gate voltages, V_{BG} and V_{TG} . The main diagonal feature in this plot corresponds to the charge neutrality point (CNP) of the graphene reservoirs. Near this reservoir CNP line, an array of steeper vertical features strongly controlled by V_{BG} arise from conductance fluctuations in the dot. Owing to our device structure, it is expected that the GQD is more strongly coupled to the bottom gate than the top gates, although the GQD is weakly influenced by the top gates due to fringing electric fields. Line cuts of the dot conductance in Fig. 1(b) highlight these features, which resemble previous studies of etched GQDs [8,36]. We also observe that the R_{dot} is maximized (~ 100 k Ω) when both the reservoirs and the GQD are at their respective CNPs. We can identify four different segmented regions bounded by the CNP lines of the reservoirs and GQD in the $V_{\text{BG}}-V_{\text{TG}}$ plane. Generally we find R_{dot} is larger in the *n-p-n* (reservoirs *n*-doped and GQD *p*-doped) or *p-n-p* regimes compared to *n-n-n* and *p-p-p* regimes due to the reduced coupling of GQD to the reservoirs when their charge carrier polarities are opposite.

A histogram of conductance minima spacing in the *n-p-n* regime [Fig. 1(c)] shows better resemblance to Gaussian than Poissonian statistics, suggesting chaotic dynamics [8,37]. Figure 1(d) shows a bias voltage (V_{dc}) and gate voltage dependent conductance map in a suppressed conductance region of Fig. 1(b), where the GQD is near its CNP while the reservoirs are *n*-doped. We find the conductance in this stability diagram remains finite and lacks sharp Coulomb blockade features, suggesting the charging energy of the GQD is much smaller than the experimental base temperature of 350 mK. This is consistent with our design parameters for the device.

Upon applying a strong perpendicular magnetic field, B , the wide graphene reservoir regions show a robust onset of the quantum Hall (QH) effect (see the Supplemental Material, Sec. II for reservoir measurements and additional data at lower magnetic field) [15]. We use the QH edge

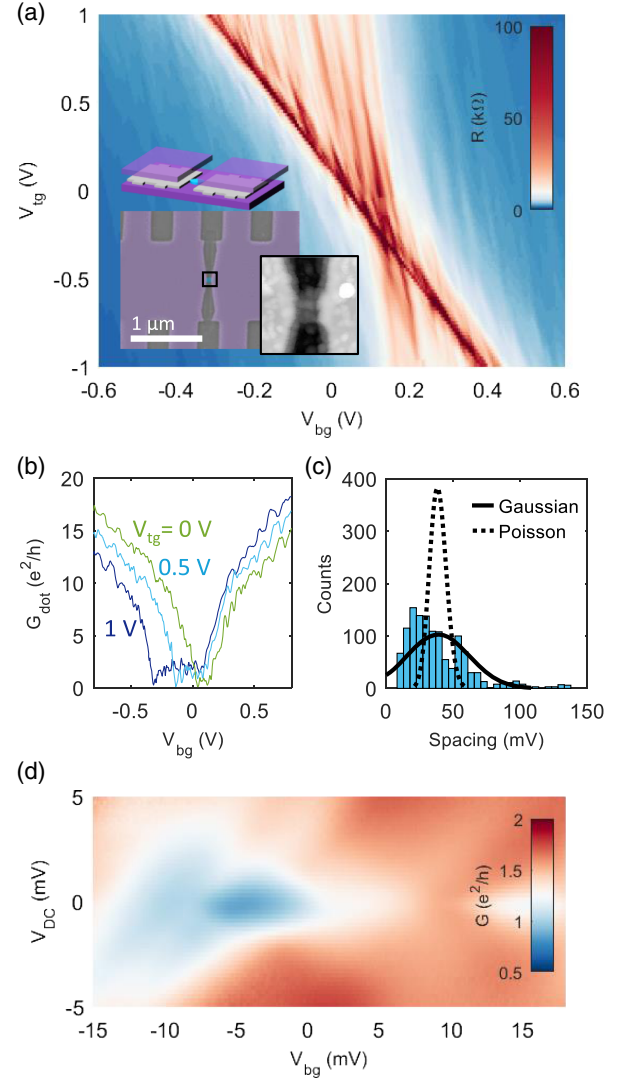


FIG. 1. (a) R_{dot} as a function of V_{BG} and V_{TG} at zero applied magnetic field, $T_{\text{bath}} = 350$ mK, and $V_{\text{Si}} = 28$ V. Inset, above: schematic of dot device with continuous bottom graphite gate (purple), GQD (blue) connected to larger reservoirs (gray), and separate top graphite gates above each reservoir. Below: scanning electron microscope image of dot device and atomic force microscope image of the GQD region. (b) G_{dot} as a function of V_{BG} at $V_{\text{TG}} = 1$ V (dark blue), 0.5 V (light blue), and 0 V (green). (c) histogram of spacing between G_{dot} minima, with fits of Poisson distribution (dashed line) and Gaussian distribution (dashed line). (d) G_{dot} as a function of V_{BG} and dc bias V_{dc} at $B = 0$ T and $V_{\text{TG}} = 0.5$ V.

states in the reservoir regions to deliver charge current I to the GQD. As shown in the insets of Fig. 2(a), we measure the longitudinal (transverse) voltage V_{xx} (V_{xy}). The upper and lower panels of Fig. 2(a) show the corresponding longitudinal (transverse) conductance $G_{xx} = I/V_{xx}$ ($G_{xy} = I/V_{xy}$) as a function of V_{BG} . Here, we keep the graphene reservoirs at constant filling fraction $\nu = 2$ by adjusting the top and bottom gate voltages simultaneously.

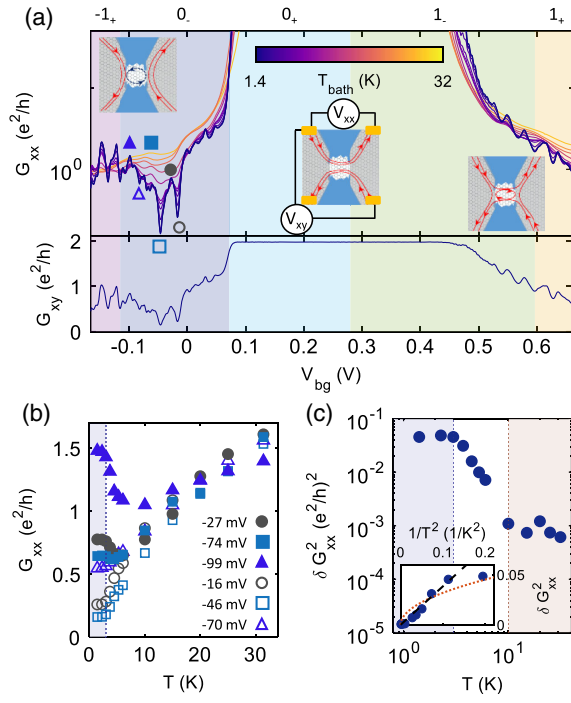


FIG. 2. (a) Upper panel: G_{xx} at $B = 10$ T with V_{BG} and V_{TG} simultaneously varied to maintain $\nu_{res} = 2$, at a range of temperatures between 1.4 K and 32 K as indicated by the color scale. Shaded regions show the doping regions for various Landau levels in the dot. Inset schematics illustrate the general behavior of the edge states in different doping regions, as well as the voltages measured to determine G_{xy} and G_{xx} without changing the polarity of the magnetic field. Open symbols mark minima plotted in (b). Lower panel: G_{xy} measured along the same V_{BG} and V_{TG} values as G_{xx} at $T = 1.41$ K. (b) The three lowest minima (open symbols) and nearby peaks (filled symbols) of G_{xx} in the $n = 0$ Landau level at $B = 10$ T as a function of temperature. Blue dashed line marks transition out of low-temperature saturation regime at T_1 . (c) Variance of G_{xx} in n_- Landau level at $B = 10$ T. Blue dashed line marks T_1 , while orange dashed line marks T_2 . Inset: variance of G_{xx} versus $1/T^2$. Black dashed line and orange dotted line show $1/T^2$ and $1/T$ fits, respectively, for $T > 3$ K.

In these measurements, we observe three principal zones of behavior: (1) suppressed conductance when the dot and reservoirs have opposite carrier types (i.e., n - p - n or p - n - p regimes); (2) full transmission of integer QH edge states [i.e., the GQD is in $\nu_{dot} = 2$ QH regime, resulting in $G_{xy} = 2e^2/h$ in Fig. 2(a)]; and (3) reentrance of finite conductance fluctuations where $\nu_{dot} > 2$. Combining this gate-dependent transport data with the TEP measured across the GQD [see Fig. 4(a), which will be discussed later], we can identify the gate voltage regions corresponding to the LL specified by n_{\pm} , where n is the LL index and subscript $+$ ($-$) corresponds to the electron (hole) side of the LL.

Since the LL filling fraction of the graphene reservoir regions is kept at $\nu_{res} = 2$, the GQD is weakly coupled to graphene electrodes for $\nu_{dot} < \nu_{res}$. This condition prevents the highly conductive QH edge states from shorting the

graphene reservoirs, allowing us to study charge transport through the GQD. The QH edge states in the reservoir serve as few-mode FL electrodes, tunnel coupled to the GQD. Employing a small number of FL modes to probe the GQD is important for preserving signatures of SYK physics, as coupling an SYK dot to a large number of FL modes is predicted to disrupt the SYK phase [12,38]. In this transport regime, where the GQD filling changes from -1_+ to 0_- , we find G_{xx} exhibits large fluctuations as V_{BG} is changed. As the temperature increases, these fluctuations diminish toward a smoothly and slowly varying background value, as shown in the upper panel of Fig. 2(a). To highlight the temperature-dependent electrical conductance changes in the SYK transport regime, Fig. 2(b) shows the temperature dependence of local extrema of $G_{xx}(V_{BG})$ in the GQD 0_- regime, with specific minima (maxima) marked by open (closed) symbols in Fig. 2(a). We find that the temperature dependence of the local minima of G_{xx} is nearly flat for temperature $T < 3$ K, then linearly increasing at higher temperatures. Local conductance maxima in the same transport regime similarly show nearly constant magnitudes up to ~ 3 K, drop toward the values of the minima as temperature increases to ~ 10 K, and increase approximately linearly as the temperature increases further.

To quantify the temperature dependence of the GQD conductance fluctuations, we study the variance of the conductance δG_{xx}^2 within transport regime 0_- after subtracting the broadly modulated baseline value. Figure 2(c) shows δG_{xx}^2 in the temperature range between 1.4 K and 30 K. This analysis highlights two relevant transition temperatures identified in the behavior of $G_{xx}(T)$ discussed above: while in the low temperature limit $T < T_1 \approx 3$ K, $\delta G_{xx}^2(T)$ is nearly constant, for $T_1 < T < T_2 \approx 10$ K, $\delta G_{xx}^2(T)$ decreases rapidly, and then less steeply for $T > T_2$.

Recent theoretical work [7,11] has predicted strong suppression of $\delta G_{xx}^2(T)$ in SYK QDs coupled to FL reservoirs. In the presence of single-particle hopping energy t between the localized states, SYK physics can be realized when the temperature is smaller than the coherence energy $E_{coh} = t^2/J$, where J is the strength of all-to-all interactions in the SYK dot. Here, the theory for reservoirs coupled to all internal GQD states predicts $\delta G_{xx}^2 \sim T^{-1}$ for $k_B T \ll E_{coh}$, crossing over to $\delta G_{xx}^2 \sim T^{-2}$ for $k_B T \gg E_{coh}$ [11]. As shown in Fig. 2(c), the experimentally observed variance exhibits $\delta G_{xx}^2 \lesssim T^{-2}$ at higher temperatures (black dashed line in inset shows T^{-2} scaling) before saturating in the low-temperature limit. The rapid decrease of the conductance fluctuations that we observe is a potential hallmark of SYK dynamics in the GQD, although the exact predicted temperature dependence is contingent on the coupling between the GQD and the reservoirs [11,12].

The strong suppression of conductance fluctuations in the GQD described above spurs us to investigate its thermoelectric response in similar transport regimes, in

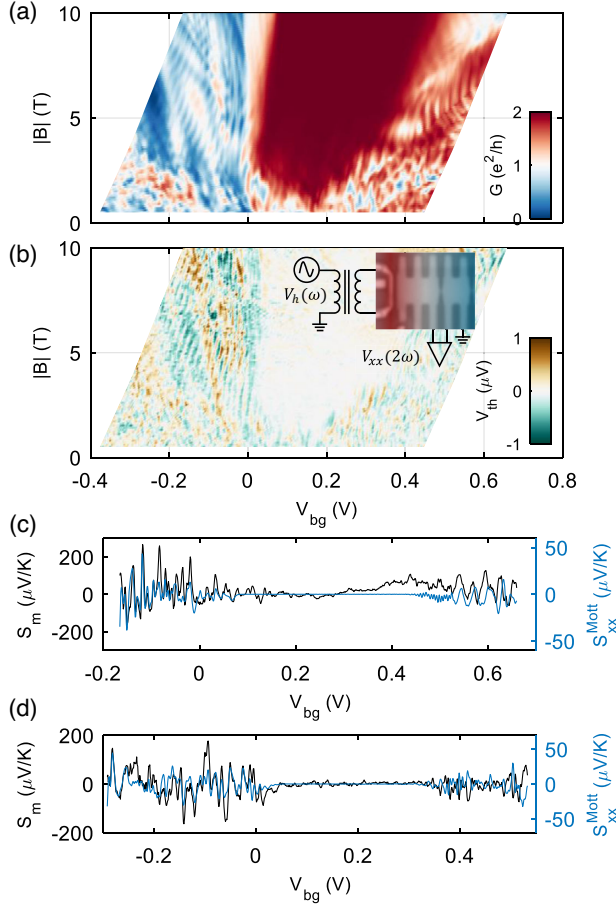


FIG. 3. (a) Evolution of G_{xy} at $T_{bath} = 3$ K as a function of V_{BG} and B , with V_{TG} simultaneously varied to keep the reservoirs at constant filling $\nu_{res} = 2$. (b) Evolution of thermally induced voltage V_{th} with the same experimental parameters as (a), using constant heater voltage $V_h = 0.3$ V. Inset: schematic of TEP measurement circuit overlaid on optical image of device. (c) Comparison line scans of S_m (black, left y axis) and Mott formula calculation (blue, right y axis) along $\nu_{res} = 2$ line at $B = 10$ T, $T = 3$ K. (d) Same comparison as (c), but at $B = 4$ T, with corresponding shift of the gate voltage values to maintain $\nu_{res} = 2$.

search of a more distinctive signature of the emergence of SYK physics [10,11,39]. Here, we apply an ac bias $V_h(\omega)$ at frequency ω to a substrate heater at the edge of one of the graphene reservoirs [inset of Fig. 3(b)]. The heating current generates a temperature gradient across the device modulated at frequency 2ω . By measuring the voltage response across the GQD at frequency 2ω , we obtain the thermoelectric voltage $V_{th} = \sqrt{2}V_{xx}(2\omega)$ in response to the temperature difference ΔT across the GQD. Figures 3(a) and 3(b) provide a comparison of the magnetic field dependence of G_{xy} (measured in the center of the $\nu_{res} = 2$ plateau at each field) with the thermally induced voltage V_{th} . In the magnetic field-dependent G_{xy} measurement [Fig. 3(a)], both reservoir edge states are transmitted through the GQD in a wide range of densities down to

$|B| \sim 3$ T. The n - p - n and n - n - n regimes show shifting patterns of oscillations as a function of B and the carrier density in the GQD, reminiscent of previous studies of larger quantum Hall p - n and n - p - n junctions [34,35,40–42]. At lower magnetic fields, the region of maximal conductance through the dot shrinks, and the transport becomes completely dominated by fluctuations. The thermally induced voltage V_{th} measured under the same conditions [Fig. 3(b)] exhibits many similar features, suggesting a strong correlation between the conductance and TEP in the GQD.

To obtain the TEP of the dot, $S_m = -V_{th}/\Delta T$, we need to estimate ΔT across the GQD for a given heater bias V_h . We employ temperature-dependent R_{xx} minima in the QH regime, measured at a pair of contacts in the graphene reservoirs. The minima of R_{xx} are lifted as a function of the thermal bath temperature T_{bath} and V_h , which allow us to estimate the temperature difference ΔT across the GQD, after considering the device geometry (see the Supplemental Material, Sec. III for details [15]).

As a benchmark, we compare the measured TEP with a generalized version of the conventional Mott formula [20],

$$S_{ij}^{Mott} = -\frac{\pi^2 k_B^2}{3e} T G_{il}^{-1} \left[\frac{\partial G_{lj}}{\partial \mu} \right], \quad (1)$$

where G_{ij} is the electrical conductance tensor and μ is the chemical potential. At $B = 10$ T [Fig. 3(c)], these quantities are broadly similar, but their magnitudes differ significantly. There is greater qualitative resemblance at lower magnetic field $B = 4$ T [Fig. 3(d)], but the magnitudes of S_m are larger than S_{xx}^{Mott} .

An important contributing factor to the magnitude discrepancy is likely that ΔT is calculated based on measurements of the nearest pair of voltage leads in the two reservoirs, which is necessarily larger than the temperature gradient across the dot itself. In contrast, V_{th} arises almost entirely in the dot, since the reservoirs are kept at $\nu_{res} = 2$, which does not contribute to the TEP in this experimental configuration [19,20,23,43]. As such, it is to be expected that S_m overestimates the true TEP of the GQD. For these reasons, our observation $|S_m| > |S_{xx}^{Mott}|$ is consistent with expectations. In the following analysis, we discuss trends in the TEP that are not impacted by questions of geometric rescaling.

Examining the temperature-dependent TEP reveals many of the similar relevant energy scales and regimes of behavior as we observe in the electrical conductance. Figure 4(a) shows $S_m(T)$ as a function of V_{BG} at $B = 10$ T, at temperatures between 1.4 and 32 K. In the low temperature limit, S_m follows the same gate dependence trend as S_{xx}^{Mott} , as discussed above. Particularly, $S_m \approx 0$ in the region $0.1 < V_{BG} < 0.4$ V. This gate range is where we observe $G_{xy} = 2e^2/h$, indicating both the GQD and graphene reservoirs are in the $\nu = 2$ QH state. Vanishing TEP in

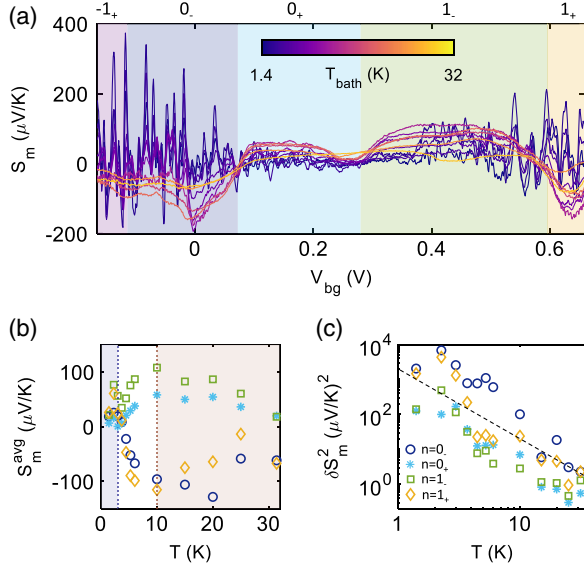


FIG. 4. (a) TEP S_m at $B = 10$ T with $\nu_{\text{res}} = 2$ at a range of temperatures between 1.4 K and 32 K. Shading indicates doping regions for various Landau levels in the GQD as defined in Fig. 2. (b) Average value of TEP S_m^{avg} as a function of bath temperature T in the regions highlighted by colors in (a). (c) TEP variance of δS_m^2 as a function of bath temperature for the regions highlighted in (a). Dashed line shows $1/T^2$ scaling.

the regime of the QH plateau is in agreement with previous studies [19,20,23,24,44]. Outside of this QH plateau region, however, S_m and S_{xx}^{Mott} exhibit rapid oscillations. The fact that the pattern of fluctuations can be explained by Eq. (1) suggests that the resonance transport across the GQD is responsible for these rapid changes of S_m as a function of V_{BG} .

As T increases, similar to the higher-temperature behavior of G_{ij} , the fluctuations of S_m as a function of gate voltage are suppressed. In the high-temperature regime ($T \gtrsim 10$ K), $S_m \approx 0$ at half-filling of the LLs (i.e., gate voltage corresponding to the transitions between 0_- and 0_+ for $n = 0$ LL and between 1_- and 1_+ for $n = 1$ LL), due to the particle-hole symmetry across the LL in the GQD. We also observe $S_m \approx 0$ at the transition between 0_+ and 1_- for $T < 30$ K, which corresponds to the center of the well-developed QH plateau at $\nu = 2$ across the entire device. Away from these vanishing points of TEP, S_m varies smoothly. We found, however, unlike the low-temperature regime ($T \lesssim 3$ K), $S_m(V_{\text{BG}})$ does not follow the trend of $S_{xx}^{\text{Mott}}(V_{\text{BG}})$ at high temperatures ($T \gtrsim 10$ K), suggesting the breakdown of the single-particle picture described by the Mott formula (see the Supplemental Material, Sec. IV for additional data and discussion [15]).

Figure 4(b) shows $S_m^{\text{avg}}(T)$, the temperature-dependent averaged S_m within the gate voltage regions corresponding to n_{\pm} . In all gate regimes, we find that $|S_m^{\text{avg}}(T)|$ exhibits distinctively different characteristic temperature-dependent

behaviors. For $T < T_1$, $|S_m^{\text{avg}}(T)|$ changes relatively slowly as large gate-dependent fluctuations dominate, similar to the low-temperature regime of $G_{xx}(T)$ discussed previously. For $T_1 < T < T_2$, $|S_m^{\text{avg}}(T)|$ monotonically increases as T increases until it reaches the maximum value near T_2 , and then decreases slowly as temperature increases further. We further compute the variance of the TEP, δS^2 , in each sector [Fig. 4(c)]. We find that δS^2 decreases as T increases, generally consistent with $1/T^2$ scaling across the entire measured range.

The complete breakdown of the Mott formalism in the high-temperature regime, particularly the slowly decreasing $|S_m^{\text{avg}}(T)|$ we observe for $T > T_2$, is inconsistent with conventional FL physics in the GQD. Indeed, recent numerical modeling of the GQD thermoelectric properties [11] predicts that the TEP in the low-temperature FL regime transitions into the SYK regime at higher temperatures, where slowly decreasing TEP is expected. Our experimental observations bear a resemblance to these theoretical predictions, suggesting an identification of $k_B T_1$ as related to the energy scale of coupling to the reservoirs and $k_B T_2 \sim E_{\text{coh}}$. However, we note that the temperature dependence of δS^2 is inconsistent with the predictions of $1/T$ scaling in this theoretical study. Some of these discrepancies from the theory, particularly in the SYK regime, may be related to the relatively small population of SYK modes in the GQD [10]. The approximate number of localized states at $B = 10$ T is $N = BA_{\text{dot}}/\Phi_0 \approx 33$, where A_{dot} is the area of the GQD. While $N \gg 1$, it is still far from the conformal limit ($N \rightarrow \infty$), necessitating the inclusion of higher-order terms to fully account for the temperature scaling behavior, and the consideration of J/N as another relevant energy scale. It is also possible that the strength of J , which we cannot directly measure, is significantly smaller than recent theoretical assumptions [7,10,12]. In this case, the system may never access the conformal limit of the SYK model, instead inhabiting a crossover regime between Fermi liquid and SYK dynamics [45].

In conclusion, we have fabricated GQDs with suppressed single-electron charging energy. Under strong magnetic fields, edge disorder alters charge transport in the strongly correlated electronic system at elevated temperatures. We observe temperature-dependent conductance fluctuation and thermoelectric power that exhibit transitioning behaviors from the FL to the putative SYK regime. Further experimental and theoretical studies, particularly considering the effects of varied coupling between the FL leads and the GQD, may distinguish between the emergence of an SYK phase and alternative scenarios, such as disordered p - n junction network formation [40,42] in the disordered GQD under magnetic fields. For more comprehensive statistics on disorder averaging, it will be beneficial to undertake a series of similar experiments with different GQDs, complemented by extensive characterization of the temperature- and magnetic field-dependent transport

behavior. Furthermore, shot noise measurements might yield valuable insights into SYK dynamics [46]. Our Letter demonstrates the possibility of disordered GQDs as an SYK platform and provides a first step toward experimental exploration of this novel quantum phase in solid-state systems.

The authors thank Bertrand Halperin and Alexander Altland for useful discussions. The major part of the experiment was supported by DOE (DE-SC0012260). L. E. A. acknowledges support from ONR MURI (N00014-21-1-2537). K. W. and T. T. acknowledge support from the JSPS KAKENHI (Grants No. 20H00354 and No. 23H02052) and World Premier International Research Center Initiative (WPI), MEXT, Japan. H. S. and S. S. acknowledge support from U.S. National Science Foundation Grant No. DMR-2245246. A. K. was supported by the Branco Weiss Society in Science, ETH Zurich, through the grant on flat bands, strong interactions, and SYK physics, and Swiss National Science Foundation Grant No. CRSK-2_221180. This work was performed, in part, at the Center for Nanoscale Systems (CNS), a member of the National Nanotechnology Infrastructure Network, which is supported by the NSF under Grant No. ECS-0335765. CNS is part of Harvard University.

-
- [1] S. Sachdev and J. Ye, Gapless spin-fluid ground state in a random quantum Heisenberg magnet, *Phys. Rev. Lett.* **70**, 3339 (1993).
 - [2] A. Kitaev, A simple model of quantum holography (part 1), *Talk at KITP Program “Entanglement in Strongly-Correlated Quantum Matter”* (2015).
 - [3] S. Sachdev, Holographic metals and the fractionalized fermi liquid, *Phys. Rev. Lett.* **105**, 151602 (2010).
 - [4] D. Chowdhury, A. Georges, O. Parcollet, and S. Sachdev, Sachdev-Ye-Kitaev models and beyond: Window into non-Fermi liquids, *Rev. Mod. Phys.* **94**, 035004 (2022).
 - [5] M. Franz and M. Rozali, Mimicking black hole event horizons in atomic and solid-state systems, *Nat. Rev. Mater.* **3**, 491 (2018).
 - [6] A. Chen, R. Ilan, F. de Juan, D. I. Pikulin, and M. Franz, Quantum holography in a graphene flake with an irregular boundary, *Phys. Rev. Lett.* **121**, 036403 (2018).
 - [7] M. Brzezińska, Y. Guan, O. V. Yazyev, S. Sachdev, and A. Kruchkov, Engineering SYK Interactions in disordered graphene flakes under realistic experimental conditions, *Phys. Rev. Lett.* **131**, 036503 (2023).
 - [8] L. A. Ponomarenko, F. Schedin, M. I. Katsnelson, R. Yang, E. W. Hill, K. S. Novoselov, and A. K. Geim, Chaotic Dirac Billiard in graphene quantum dots, *Science* **320**, 356 (2008).
 - [9] S. Engels, A. Epping, C. Volk, S. Korte, B. Voigtlander, K. Watanabe, T. Taniguchi, S. Trellenkamp, and C. Stampfer, Etched graphene quantum dots on hexagonal boron nitride, *Appl. Phys. Lett.* **103**, 073113 (2013).
 - [10] A. Kruchkov, A. A. Patel, P. Kim, and S. Sachdev, Thermoelectric power of Sachdev-Ye-Kitaev islands: Probing Bekenstein-Hawking entropy in quantum matter experiments, *Phys. Rev. B* **101**, 205148 (2020).
 - [11] H. Shackleton, L. E. Anderson, P. Kim, and S. Sachdev, Conductance and thermopower fluctuations in interacting quantum dots, *Phys. Rev. B* **109**, 235109 (2024).
 - [12] O. Can, E. M. Nica, and M. Franz, Charge transport in graphene-based mesoscopic realizations of Sachdev-Ye-Kitaev models, *Phys. Rev. B* **99**, 045419 (2019).
 - [13] C. R. Dean, A. F. Young, I. Meric, C. Lee, L. Wang, S. Sorgenfrei, K. Watanabe, T. Taniguchi, P. Kim, K. L. Shepard, and J. Hone, Boron nitride substrates for high-quality graphene electronics, *Nat. Nanotechnol.* **5**, 722 (2010).
 - [14] L. Wang, I. Meric, P. Y. Huang, Q. Gao, Y. Gao, H. Tran, T. Taniguchi, K. Watanabe, L. M. Campos, D. A. Muller, J. Guo, P. Kim, J. Hone, K. L. Shepard, and C. R. Dean, One-dimensional electrical contact to a two-dimensional material, *Science* **342**, 614 (2013).
 - [15] See Supplemental Material at <http://link.aps.org/supplemental/10.1103/PhysRevLett.132.246502>, which includes Refs. [16–35], for discussion of fabrication methods, measurement techniques, and additional data.
 - [16] A. Cheng, T. Taniguchi, K. Watanabe, P. Kim, and J.-D. Pilllet, Guiding Dirac fermions in graphene with a carbon nanotube, *Phys. Rev. Lett.* **123**, 216804 (2019).
 - [17] S. Datta, *Electronic Transport in Mesoscopic Systems*, 1st ed. (Cambridge University Press, Cambridge, England, 1995).
 - [18] K. Zimmermann, A. Jordan, F. Gay, K. Watanabe, T. Taniguchi, Z. Han, V. Bouchiat, H. Sellier, and B. Sécépé, Tunable transmission of quantum Hall edge channels with full degeneracy lifting in split-gated graphene devices, *Nat. Commun.* **8**, 14983 (2017).
 - [19] F. Ghahari Kermani, Interaction Effects on Electric and Thermoelectric Transport in Graphene, Ph.D. thesis, Columbia University, 2014.
 - [20] Y. M. Zuev, W. Chang, and P. Kim, Thermoelectric and magnetothermoelectric transport measurements of graphene, *Phys. Rev. Lett.* **102**, 096807 (2009).
 - [21] A. J. M. Giesbers, U. Zeitler, M. I. Katsnelson, L. A. Ponomarenko, T. M. Mohiuddin, and J. C. Maan, Quantum-hall activation gaps in graphene, *Phys. Rev. Lett.* **99**, 206803 (2007).
 - [22] A. T. Pierce, Y. Xie, S. H. Lee, P. R. Forrester, D. S. Wei, K. Watanabe, T. Taniguchi, B. I. Halperin, and A. Yacoby, Thermodynamics of free and bound magnons in graphene, *Nat. Phys.* **18**, 37 (2022).
 - [23] J. G. Checkelsky and N. P. Ong, Thermopower and Nernst effect in graphene in a magnetic field, *Phys. Rev. B* **80**, 081413(R) (2009).
 - [24] F. Ghahari, H. Y. Xie, T. Taniguchi, K. Watanabe, M. S. Foster, and P. Kim, Enhanced thermoelectric power in graphene: Violation of the Mott relation by inelastic scattering, *Phys. Rev. Lett.* **116**, 136802 (2016).
 - [25] N. W. Ashcroft and M. N. David, *Solid State Physics*, college ed. (Harcourt College Publishers, New York, 1976), pp. 256–259.
 - [26] M. Jonson and S. M. Girvin, Thermoelectric effect in a weakly disordered inversion layer subject to a quantizing magnetic field, *Phys. Rev. B* **29**, 1939 (1984).

- [27] H. Obloh, K. V. Klitzing, and K. Ploog, Thermopower measurements on the two-dimensional electron gas of GaAs – $\text{Al}_x\text{Ga}_{1-x}\text{As}$ heterostructures, *Surface Sci.* **142**, 236 (1984).
- [28] R. Fletcher, J. C. Maan, and G. Weimann, Experimental results on the high-field thermopower of a two-dimensional electron gas in a GaAs – $\text{Ga}_{1-x}\text{Al}_x\text{As}$ heterojunction, *Phys. Rev. B* **32**, 8477(R) (1985).
- [29] C. Ruf, H. Obloh, B. Junge, E. Gmelin, K. Ploog, and G. Weimann, Phonon-drag effect in GaAs – $\text{Al}_x\text{Ga}_{1-x}\text{As}$ heterostructures at very low temperatures, *Phys. Rev. B* **37**, 6377 (1988).
- [30] K. I. Bolotin, F. Ghahari, M. D. Shulman, H. L. Stormer, and P. Kim, Observation of the fractional quantum Hall effect in graphene, *Nature (London)* **462**, 196 (2009).
- [31] D. K. Efetov and P. Kim, Controlling electron-phonon interactions in graphene at ultrahigh carrier densities, *Phys. Rev. Lett.* **105**, 256805 (2010).
- [32] Y. M. Zuev, Nanoscale Thermoelectric Energy Conversion, Ph.D. thesis, Columbia University, 2011.
- [33] C. W. J. Beenakker and A. A. M. Staring, Theory of the thermopower of a quantum dot, *Phys. Rev. B* **46**, 9667 (1992).
- [34] D. A. Abanin and L. S. Levitov, Quantized transport in graphene p-n junctions in a magnetic field, *Science* **317**, 641 (2007).
- [35] B. Özyilmaz, P. Jarillo-Herrero, D. Efetov, D. A. Abanin, L. S. Levitov, and P. Kim, Electronic transport and quantum hall effect in bipolar graphene p-n-p junctions, *Phys. Rev. Lett.* **99**, 166804 (2007).
- [36] J. Güttinger, C. Stampfer, F. Libisch, T. Frey, J. Burgdörfer, T. Ihn, and K. Ensslin, Electron-hole crossover in graphene quantum dots, *Phys. Rev. Lett.* **103**, 046810 (2009).
- [37] L. Huang, Y. C. Lai, and C. Grebogi, Characteristics of level-spacing statistics in chaotic graphene billiards, *Chaos* **21**, 013102 (2011).
- [38] S. Banerjee and E. Altman, Solvable model for a dynamical quantum phase transition from fast to slow scrambling, *Phys. Rev. B* **95**, 134302 (2017).
- [39] R. A. Davison, W. Fu, A. Georges, Y. Gu, K. Jensen, and S. Sachdev, Thermoelectric transport in disordered metals without quasiparticles: The Sachdev-Ye-Kitaev models and holography, *Phys. Rev. B* **95**, 155131 (2017).
- [40] D. S. Wei, T. van der Sar, S. H. Lee, K. Watanabe, T. Taniguchi, B. I. Halperin, and A. Yacoby, Electrical generation and detection of spin waves in a quantum Hall ferromagnet, *Science* **362**, 229 (2018).
- [41] J. R. Williams, L. DiCarlo, and C. M. Marcus, Electrical generation and detection of spin waves in a quantum Hall ferromagnet, *Science* **317**, 638 (2007).
- [42] K. Wang, A. Harzheim, T. Taniguchi, K. Watanabe, J. U. Lee, and P. Kim, Tunneling spectroscopy of quantum hall states in bilayer graphene p-n junctions, *Phys. Rev. Lett.* **122**, 146801 (2019).
- [43] W. Duan, J. F. Liu, C. Zhang, and Z. Ma, Thermoelectric and thermal transport properties of graphene under strong magnetic field, *Physica E (Amsterdam)* **104**, 173 (2018).
- [44] P. Wei, W. Bao, Y. Pu, C. N. Lau, and J. Shi, Anomalous thermoelectric transport of dirac particles in graphene, *Phys. Rev. Lett.* **102**, 166808 (2009).
- [45] A. Altland, D. Bagrets, and A. Kamenev, Sachdev-Ye-Kitaev non-fermi-liquid correlations in nanoscopic quantum transport, *Phys. Rev. Lett.* **123**, 226801 (2019).
- [46] A. Nikolaenko, S. Sachdev, and A. A. Patel, Theory of shot noise in strange metals, *Phys. Rev. Res.* **5**, 043143 (2023).